Quantum interference between nuclear excitation by electron capture and radiative recombination

Adriana Pálffy,[1,*] Zoltán Harman,[2,†] and Werner Scheid[1]
[1]*Institut für Theoretische Physik, Justus-Liebig-Universität Giessen, Heinrich-Buff-Ring 16, 35392 Giessen, Germany*
[2]*Max-Planck-Institut für Kernphysik, Saupfercheckweg 1, 69117 Heidelberg, Germany*
(Received 6 October 2006; published 11 January 2007)

We investigate the quantum interference between the resonant process of nuclear excitation by electron capture (NEEC) followed by the radiative decay of the excited nucleus, and radiative recombination (RR). In order to derive the interference cross section, a Feshbach projection operator formalism is used. The electromagnetic field is considered by means of multipole fields. The nucleus is described by a phenomenological collective model and by making use of experimental data. The Fano profile parameters as well as the interference cross section for electric and magnetic multipole transitions in various heavy ions are presented. We discuss the experimental possibility of discerning NEEC from the RR background.

DOI: 10.1103/PhysRevA.75.012709 PACS number(s): 34.80.Lx, 23.20.Nx, 23.20.−g

I. INTRODUCTION

The process of photorecombination in highly charged heavy ions has been the subject of many theoretical and experimental studies up to today, concerning both radiative recombination (RR) and dielectronic recombination (DR) (see, e.g., Refs. [1,2]) and their interference. With the enhanced experimental possibilities and achieved precision, the subject of electron recombination into highly charged ions has been expanding to include quantum electrodynamics (QED) corrections [3]. The effect of interference between RR with DR has been theoretically studied (see, e.g., Ref. [4]) and experimentally concluded [2,5,6].

In Ref. [7] a recombination process that is the nuclear analog of DR has been theoretically proposed. Although not yet experimentally observed, nuclear excitation by electron capture (NEEC) has been an interesting subject after experimental observations of atomic physics processes with regard to the structure of the nucleus have been recently reported, such as bound-state internal conversion [8] and nuclear excitation by electron transition (NEET) [9]. In the resonant process of NEEC, a free electron is recombined into a bound state of an ion with the simultaneous excitation of the nucleus. The excited nucleus can then decay radiatively or by internal conversion. Several theoretical studies have been made concerning NEEC in plasmas [7,10] or in solid targets [11–13]. In Ref. [14] we presented relativistically correct theoretical cross sections for NEEC followed by the radiative decay of the nuclear excited states for highly charged heavy ions.

If the initial and final states for NEEC and RR coincide, quantum interference between the two processes occurs. Such an interference effect is interesting as it involves two very different pathways: while in RR only the recombining electron is involved, NEEC corresponds to a quantum path in which the nucleus is excited. In Fig. 1 the RR and NEEC mechanisms are shown schematically. In addition to NEEC, the strong competing process of RR is always present in an experiment. Therefore, the magnitude of the interference effect may also play an important role for observing NEEC.

In this paper we theoretically investigate the interference between NEEC and RR, focusing on collision systems with suitable excitation energies that could be candidates for experimental observation. We derive the total cross section of the recombination process with the help of a Feshbach projection operator formalism, which allows the separation of the interference term from the NEEC and RR cross sections. The radiation field is expanded in terms of multipoles in order to clearly discern the NEEC transition multipolarities. The electric and magnetic electron-nucleus interactions are considered explicitly, and the nucleus is described with the help of a geometrical collective model and making use of experimental data. The dynamics of the electron is governed by the Dirac equation. We express the interference term of the cross section using the dimensionless Fano profile parameter for electric and magnetic transitions in Sec. II. The numerical results of the calculation are given in Sec. III, together with an interpretation of the results regarding the possibility of an experimental observation of NEEC. We conclude with a short summary. In this work atomic units are used unless otherwise specified.

II. THEORETICAL FORMALISM FOR INTERFERENCE EFFECTS

In this section we derive the total cross section of the recombination process involving NEEC followed by the radiative decay of the nucleus and RR by means of a Feshbach projection operator formalism. We consider that the electron is captured into the bound state of a bare ion or an ion with a closed-shell configuration. We calculate the interference term between NEEC followed by the radiative decay of the excited nucleus and RR in the total cross section for electric and magnetic multipole transitions of the nucleus.

A. The interference between RR and NEEC in the total cross section

The initial state $|\Psi_i\rangle$ of the system describing the nucleus in its ground state, the free electron, and the vacuum state of

*Electronic address: Adriana-Claudia.Gagyi-Palffy@uni-giessen.de
†Electronic address: Harman@mpi-hd.mpg.de

the electromagnetic field can be written as a direct product of the nuclear, electronic, and photonic state vectors:

$$|\Psi_i\rangle = |NI_iM_{I_i},\vec{p}m_s,0\rangle \equiv |NI_iM_{I_i}\rangle \otimes |\vec{p}m_s\rangle \otimes |0\rangle. \quad (1)$$

Here, $\vec{p}$ is the asymptotic momentum of the electron, m_s its spin projection, and $|N\rangle$ the nuclear ground state, denoted by the total angular momentum I_i and its projection M_{I_i}. In considering RR or NEEC followed by the radiative decay of the nucleus, the final state of the recombined system $|\Psi_f\rangle$ consists of the nucleus in its ground state, the bound electron and the emitted photon. Rather than using the plane wave expansion for the electromagnetic field as in Ref. [14], it is more convenient in this case to consider photons of a given angular momentum and parity. The final state can be written as

$$|\Psi_f\rangle = |NI_fM_{I_f},n_f\kappa_fm_f,\lambda kLM\rangle \equiv |NI_fM_{I_f}\rangle \otimes |n_f\kappa_fm_f\rangle \otimes |\lambda kLM\rangle, \quad (2)$$

with n_f, κ_f, and m_f being the principal, Dirac angular momentum, and magnetic quantum numbers of the bound one-electron state, respectively. The emitted photon has the wave number k, the total angular momentum L and its projection M. Furthermore, λ stands for electric (e) or magnetic (m) waves. The intermediate resonant state formed by the electron capture in the process of NEEC consists of the excited nucleus, the bound electron, and the vacuum state of the electromagnetic field

$$|\Psi_d\rangle = |N^*I_dM_{I_d},n_d\kappa_dm_d,0\rangle \equiv |N^*I_dM_{I_d}\rangle \otimes |n_d\kappa_dm_d\rangle \otimes |0\rangle. \quad (3)$$

The excited nuclear state is denoted by $|N^*\rangle$. In our case, the recombined electron does not undergo further decay cascades, i.e., $n_d=n_f$, $\kappa_d=\kappa_f$, and $m_d=m_f$.

Following the formalism presented in Ref. [14], we introduce projector operators onto the individual subspaces, in order to separate these states in the perturbative expansion of the transition operator. We neglect corrections due to two or more photon states [15,16] and due to the presence of the negative electronic continuum. The Fock space is then given by the sum of three subspaces: the subspace of the states that contain the free electron, with its projector operator P, the subspace of the states characterized by the presence of the excited nucleus, together with the corresponding projector operator Q, and finally the subspace of the states with a photon, associated with the projector operator R. We postulate the completeness relation

$$P + Q + R = \mathbf{1}, \quad (4)$$

where $\mathbf{1}$ is the unity operator of the total Fock space.

The total Hamiltonian operator for the system consisting of the nucleus (n), the electron (e), and the radiation field (r) can be written as

$$H = H_n + H_e + H_r + H_{en} + H_{er} + H_{nr}. \quad (5)$$

The expressions of the first three Hamiltonians can be found in Ref. [14]. Interactions between the three subsystems are described by the three remaining Hamiltonians in Eq. (5). We

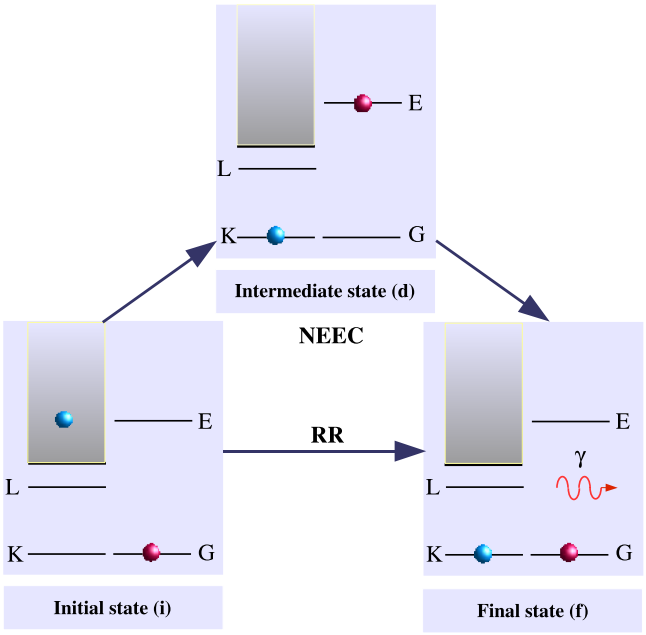

FIG. 1. (Color online) NEEC and RR recombination mechanisms of a continuum electron into the K shell of a bare ion. The nucleus is schematically represented as undergoing the transition from the ground state (G) to the excited state (E) and again to its ground state.

adopt the Coulomb gauge for the electron-nucleus interaction (en) because it allows the separation of the dominant Coulomb attraction between the electronic and the nuclear degrees of freedom:

$$H_{en} = \int d^3r_n \frac{\rho_n(\vec{r}_n)}{|\vec{r}_e - \vec{r}_n|}. \quad (6)$$

Here, $\rho_n(\vec{r}_n)$ is the nuclear charge density and the integration is performed over the whole nuclear volume. The static part of the electron-nucleus interaction is contained in the Hamiltonian H_e. The interaction of the electron with the transverse photon field quantized in the volume of a sphere of radius R is given by

$$H_{er} = -\vec{\alpha}\cdot\vec{A} = -\sum_{\lambda kLM}\left[a^\dagger_{\lambda kLM}\vec{\alpha}\cdot\vec{A}_{\lambda kLM}(\vec{r}) + \text{H . c .}\right], \quad (7)$$

with the vector potential of the quantized electromagnetic field [17]

$$\vec{A}(\vec{r}) = \sum_{\lambda kLM}\left[\vec{A}_{\lambda kLM}(\vec{r})a^\dagger_{\lambda kLM} + \vec{A}^*_{\lambda kLM}(\vec{r})a_{\lambda kLM}\right]. \quad (8)$$

Here, $\vec{\alpha}$ is the vector of the Dirac matrices and the two independent solutions of the wave equation for the $\vec{A}_{\lambda kLM}(\vec{r})$ are

$$\vec{A}_{(m)kLM}(\vec{r}) = \sqrt{\frac{4\pi ck}{R}} j_L(kr)\vec{Y}^M_{LL}(\theta,\varphi),$$

$$\vec{A}_{(e)kLM}(\vec{r}) = \frac{i}{k}\sqrt{\frac{4\pi ck}{R}}\vec{\nabla}\times[j_L(kr)\vec{Y}^M_{LL}(\theta,\varphi)], \tag{9}$$

where the wave number k is discretized by requiring the proper boundary conditions at a perfectly conducting sphere of radius R. In Eq. (9), $j_L(kr)$ stands for the spherical Bessel function. The $\vec{Y}^M_{LL}(\theta,\varphi)$ denote the vector spherical harmonics, given by [18]

$$\vec{Y}^M_{LL}(\theta,\varphi) = \sum_{\nu}\sum_{q} C(L1L;\nu qM)Y_{L\nu}(\theta,\varphi)\vec{\epsilon}_q, \tag{10}$$

where $q=0,\pm 1$ and the spherical unit vectors $\vec{\epsilon}_q$ expressed in terms of the Cartesian unit vectors $(\vec{e}_x,\vec{e}_y,\vec{e}_z)$ are

$$\vec{\epsilon}_+ = -\frac{1}{\sqrt{2}}(\vec{e}_x + i\vec{e}_y),$$

$$\vec{\epsilon}_0 = \vec{e}_z,$$

$$\vec{\epsilon}_- = \frac{1}{\sqrt{2}}(\vec{e}_x - i\vec{e}_y). \tag{11}$$

Similarly, the interaction of the nucleus with the electromagnetic field is given by the Hamiltonian

$$H_{nr} = -\frac{1}{c}\sum_{\lambda kLM}\left[a^\dagger_{\lambda kLM}\int d^3r_n\vec{j}_n(\vec{r}_n)\cdot\vec{A}_{\lambda kLM}(\vec{r}_n) + \text{H . c .}\right], \tag{12}$$

where $\vec{j}_n(\vec{r}_n)$ is the nuclear current.

Using the projection operators we can separate the perturbation V in the total Hamiltonian

$$H = H_0 + V, \tag{13}$$

with

$$H_0 = PHP + QHQ + RHR, \tag{14}$$

$$V \equiv H - H_0 = PHQ + QHP + PHR + RHP + RHQ + QHR. \tag{15}$$

This way of defining H_0 has the advantage that the effect of the nuclear potential on bound and continuum electron states is included in H_0 to all orders. The individual terms in the perturbation operator describe transitions between the different subspaces. For example, QHP describes in the lowest order the time-reversed process of internal conversion (IC), namely, NEEC, while PHR and RHP are the first-order operators for photoionization and radiative recombination, respectively.

The transition operator is defined as [19]

$$T(z) = V + VG(z)V, \tag{16}$$

where $G(z)$ is the Green operator of the total system given by

$$G(z) = (z - H)^{-1}. \tag{17}$$

Here, z is a complex energy variable. The total cross section for a process can be expressed by the modulus square of the matrix element of the transition operator, after summing over the final states and averaging over the initial states that are not resolved in the experiment,

$$\sigma_{i\to f}(E) = \frac{2\pi}{F_i}\sum_{M_{I_f}m_d}\sum_{\lambda LM}\frac{1}{2(2I_i+1)}\sum_{M_{I_i}m_s}\frac{1}{4\pi} \times\int d\Omega_p \lim_{\epsilon\to 0+}|\langle\Psi_f|T(E+i\epsilon)|\Psi_i\rangle|^2\rho_f, \tag{18}$$

with the Ψ_f and Ψ_i as final and initial eigenstates of H_0, respectively [see Eqs. (1) and (2)]. Here, F_i denotes the flux of the incoming electrons, ρ_f the density of the final photonic states, and Ω_p is the direction of the incoming free electron characterized by the angles θ_p and φ_p.

We use the Lippmann-Schwinger equation

$$G(z) = G_0(z) + G_0(z)VG_0(z) + G_0(z)VG_0(z)VG_0(z) + \cdots \tag{19}$$

to write the perturbation series for $T(z)$ in powers of V with the Green function $G_0(z)$ of the unperturbed Hamiltonian H_0:

$$T(z) = V + VG_0(z)V + VG_0(z)VG_0(z)V + \cdots. \tag{20}$$

Since the initial state of the NEEC process is by definition an eigenstate of P, and the final state is an eigenstate of R, we only need to consider the projection RTP of the transition operator

$$RT(z)P = RVP + RVG_0(z)VP + RVG_0(z)VG_0(z)VP + RVG_0(z)VG_0(z)VG_0(z)VP + \cdots. \tag{21}$$

The first term RVP accounts for the radiative recombination. Taking into account from the infinite perturbation expansion in Eq. (21) the terms that correspond to NEEC [14] we can write the final expression for the transition amplitude for the recombination process as

$$\langle\Psi_f|RT(z)P|\Psi_i\rangle = \langle\Psi_f|RH_{er}P|\Psi_i\rangle + \sum_d \frac{\langle\Psi_f|H_{nr}|\Psi_d\rangle\langle\Psi_d|H_{en}+H_{\text{magn}}|\Psi_i\rangle}{z - E_d + \frac{i}{2}\Gamma_d}. \tag{22}$$

Here, Γ_d denotes the total natural width of the excited state $|d\rangle = |N^*I_dM_{I_d},n_d\kappa_dm_d,0\rangle$. The magnetic interaction Hamiltonian H_{magn} accounts for the recombination of the free electron by exchanging a virtual transverse photon with the nucleus in the unretarded approximation [14]

$$H_{\text{magn}} = -\frac{1}{c}\vec{\alpha}\int d^3r_n\frac{\vec{j}_n(\vec{r}_n)}{|\vec{r}-\vec{r}_n|}. \tag{23}$$

Using the expression of the transition operator, the total cross section can then be written as

$$\sigma_{i\to f}(E) = \frac{2\pi}{F_i} \sum_{M_{I_f} m_d} \sum_{\lambda LM} \frac{1}{2(2I_i+1)} \sum_{M_{I_i} m_s} \frac{1}{4\pi} \int d\Omega_p \Bigg| \langle NI_f M_{I_f}, n_d \kappa_d m_d, \lambda k LM | H_{er} | NI_i M_{I_i}, \vec{p} m_s, 0 \rangle$$

$$+ \sum_{M_{I_d}} \frac{\langle NI_f M_{I_f}, n_d \kappa_d m_d, \lambda k LM | H_{nr} | N^* I_d M_{I_d}, n_d \kappa_d m_d, 0 \rangle}{(E - E_d) + \frac{i}{2}\Gamma_d}$$

$$\times \langle N^* I_d M_{I_d}, n_d \kappa_d m_d, 0 | H_{en} + H_{\mathrm{magn}} | NI_i M_{I_i}, \vec{p} m_s, 0 \rangle \Bigg|^2 \rho_f. \tag{24}$$

The first term in the modulus squared accounts for RR and the second one for NEEC. We can separate therefore the equation above in three terms

$$\sigma_{i\to f}(E) = \sigma_{\mathrm{RR}}(E) + \sigma_{\mathrm{NEEC}}(E) + \sigma_{\mathrm{int}}(E), \tag{25}$$

with the RR and NEEC total cross sections given by

$$\sigma_{\mathrm{RR}}(E) = \frac{2\pi}{F_i} \sum_{M_{I_f} m_d} \sum_{\lambda LM} \frac{1}{2(2I_i+1)} \sum_{M_{I_i} m_s} \frac{1}{4\pi} \int d\Omega_p |\langle NI_f M_{I_f}, n_d \kappa_d m_d, \lambda k LM | H_{er} | NI_i M_{I_i}, \vec{p} m_s, 0 \rangle|^2 \rho_f \tag{26}$$

and

$$\sigma_{\mathrm{NEEC}}(E) = \frac{2\pi}{F_i} \sum_{M_{I_f} m_d} \sum_{M_{I_d}} \sum_{\lambda LM} \frac{1}{2(2I_i+1)} \sum_{M_{I_i} m_s} \frac{1}{4\pi} \int d\Omega_p \Bigg| \frac{\langle NI_f M_{I_f}, n_d \kappa_d m_d, \lambda k LM | H_{nr} | N^* I_d M_{I_d}, n_d \kappa_d m_d, 0 \rangle}{(E - E_d) + \frac{i}{2}\Gamma_d}$$

$$\times \langle N^* I_d M_{I_d}, n_d \kappa_d m_d, 0 | H_{en} + H_{\mathrm{magn}} | NI_i M_{I_i}, \vec{p} m_s, 0 \rangle \Bigg|^2 \rho_f. \tag{27}$$

The term describing the interference between RR and NEEC can be written as

$$\sigma_{\mathrm{int}}(E) = \frac{2\pi}{F_i} \sum_{M_{I_f} m_d} \sum_{M_{I_d}} \sum_{\lambda LM} \frac{\rho_f}{2(2I_i+1)} \sum_{M_{I_i} m_s} \frac{1}{4\pi} \int d\Omega_p \Bigg(\frac{\langle NI_f M_{I_f}, n_d \kappa_d m_d, \lambda k LM | H_{nr} | N^* I_d M_{I_d}, n_d \kappa_d m_d, 0 \rangle}{(E - E_d) + \frac{i}{2}\Gamma_d}$$

$$\times \langle N^* I_d M_{I_d}, n_d \kappa_d m_d, 0 | H_{en} + H_{\mathrm{magn}} | NI_i M_{I_i}, \vec{p} m_s, 0 \rangle \langle NI_f M_{I_f}, n_d \kappa_d m_d, \lambda k LM | H_{er} | NI_i M_{I_i}, \vec{p} m_s, 0 \rangle^* + \mathrm{H.c.} \Bigg). \tag{28}$$

The aim of this paper is to calculate the interference term in the total cross section. The calculation of the NEEC cross section and predicted values for several collision systems can be found in Ref. [14]. Furthermore, the calculation of the RR total cross section is well understood. An extensive tabulation of relativistic total cross sections for RR as a function of energy ranging from closely above the threshold to the relativistic regime of relative electron energies is available in Ref. [20].

If we consider the matrix element of the Hamiltonian H_{er} connecting the radiation field and the electrons in the interference term, the initial and the final total nuclear angular momenta as well as their projections have to coincide, as they are not influenced by RR,

$$\langle NI_f M_{I_f}, n_d \kappa_d m_d, \lambda k LM | H_{er} | NI_i M_{I_i}, \vec{p} m_s, 0 \rangle = \delta_{I_i I_f} \delta_{M_{I_f} M_{I_i}} \langle n_d \kappa_d m_d, \lambda k LM | H_{er} | \vec{p} m_s, 0 \rangle. \tag{29}$$

The initial state continuum electronic wave function is given through the partial wave expansion [21]

$$|\vec{p} m_s\rangle = \sum_{\kappa m m_l} i^l e^{i\Delta_\kappa} Y^*_{l m_l}(\Omega_p) C\left(l \frac{1}{2} j; m_l m_s m \right) |\varepsilon \kappa m\rangle, \tag{30}$$

where ε is the energy of the continuum electron measured from the ionization threshold, $\varepsilon = \sqrt{p^2c^2 + c^4} - c^2$. The orbital angular momentum of the partial wave is denoted by l and the corresponding magnetic quantum number by m_l, while the partial wave phases Δ_κ are chosen so that the continuum wave function fulfills the boundary conditions of an incoming plane wave and an

outgoing spherical wave. The total angular momentum quantum number of the partial wave is $j=|\kappa|-\frac{1}{2}$. The interference cross section in the case of NEEC involving a nuclear transition with specific parity λ and multipolarity L can then be written as

$$\sigma_{\rm int} = \frac{2\pi}{F_i} \sum_{M_{I_d} M_{I_i}} \sum_{M m_d} \frac{\rho_f}{2(2I_i+1)} \sum_{\kappa m} \frac{1}{4\pi} \Bigg(\frac{\langle NI_iM_{I_i}, \lambda kLM | H_{nr} | N^* I_d M_{I_d}, 0\rangle}{(E-E_d)+\frac{i}{2}\Gamma_d} \langle N^* I_d M_{I_d}, n_d \kappa_d m_d | H_{en} + H_{\rm magn} | NI_iM_{I_i}, \varepsilon \kappa m\rangle$$
$$\times \langle n_d \kappa_d m_d, \lambda kLM | H_{er} | \varepsilon \kappa m, 0\rangle^* + \text{H . c .} \Bigg). \tag{31}$$

We can relate the interference cross section term with the NEEC cross section, introducing the dimensionless Fano profile parameter Q_f. The expression of the NEEC cross section from Ref. [14] is

$$\sigma_{\rm NEEC}(E) = \frac{2\pi^2}{p^2} \frac{A_r^{d\to f} Y_n^{i\to d}}{\Gamma_d} L_d(E-E_d), \tag{32}$$

where $A_r^{d\to f}$ is the radiative rate defined as

$$A_r^{d\to f} = \frac{2\pi}{2I_d+1} \sum_{M_{I_f} M} \sum_{M_{I_d}} |\langle NI_fM_{I_f}, n_d\kappa_d m_d, \lambda kLM | H_{nr} | N^* I_d M_{I_d}, n_d \kappa_d m_d, 0\rangle|^2 \rho_f \tag{33}$$

and $Y_n^{i\to d}$ is the NEEC rate

$$Y_n^{i\to d} = \frac{2\pi}{2(2I_i+1)} \sum_{M_{I_i} m_s} \sum_{M_{I_d} m_d} \int d\Omega_p |\langle N^* I_d M_{I_d}, n_d \kappa_d m_d, 0 | H_{en} + H_{\rm magn} | NI_iM_{I_i}, \vec{p} m_s, 0\rangle|^2 \rho_i. \tag{34}$$

Furthermore, p denotes the continuum electron momentum and ρ_i the density of the initial electronic states. The explicit energy dependence of the interference term can be expressed with the help of the Lorentz profile $L_d(E-E_d)$, defined as

$$L_d(E-E_d) = \frac{\Gamma_d/2\pi}{(E-E_d)^2 + \frac{1}{4}\Gamma_d^2}, \tag{35}$$

which in turn is related to the NEEC total cross section. The interference cross section can be written in the concise form [4]

$$\sigma_{\rm int} = \sigma_{\rm NEEC} \frac{\Gamma_d}{Y_n^{i\to d}} \frac{2I_d+1}{2I_i+1} \left[2\frac{E-E_d}{\Gamma_d} \text{Re}\left(\frac{1}{Q_f}\right) + \text{Im}\left(\frac{1}{Q_f}\right) \right], \tag{36}$$

with the inverse of the dimensionless Fano profile parameter

$$\frac{1}{Q_f} = \pi \rho_i \sum_{M_{I_d} M_{I_i}} \sum_{M m_d} \sum_{\kappa m} \langle N^* I_d M_{I_d}, n_d \kappa_d m_d | H_{en} + H_{\rm magn} | NI_iM_{I_i}, \varepsilon \kappa m\rangle$$
$$\times \frac{\langle NI_iM_{I_i}, \lambda kLM | H_{nr} | N^* I_d M_{I_d}, 0\rangle \langle n_d \kappa_d m_d, \lambda kLM | H_{er} | \varepsilon \kappa m, 0\rangle^*}{\sum_{M'_{I_i} M'} \sum_{M'_{I_d}} \left| \langle NI_iM'_{I_i}, k\lambda LM' | H_{nr} | N^* I_d M'_{I_d}, 0\rangle \right|^2}. \tag{37}$$

We have used primed indices for the summations in the expression of the nuclear radiative rate in the denominator. With the further observation that the inverse Fano profile parameter $1/Q_f$ is real for both the electric and magnetic cases, the interference cross section yields

$$\sigma_{\mathrm{int}} = \sigma_{\mathrm{NEEC}} \frac{2(E-E_d)}{Y_n^{i\to d}} \frac{2I_d+1}{2I_i+1} \frac{1}{Q_f}. \tag{38}$$

B. Electric transitions

In order to calculate the matrix elements in the Fano profile parameter in Eq. (37), an adequate nuclear model is needed. Following the outline in Ref. [14], we describe the nucleus by means of a geometrical collective model [22] which assumes that the excitations of the nucleus are vibrations and rotations of the nuclear surface, which is parametrized as

$$R(\theta,\varphi,t) = R_0\left(1 + \sum_{l=0}^{\infty} \sum_{m=-l}^{l} \alpha_{lm}^*(t) Y_{lm}(\theta,\varphi)\right). \tag{39}$$

The time-dependent deformation amplitudes $\alpha_{lm}(t)$ describe the nuclear surface with respect to a sphere of radius R_0 and serve as collective coordinates. This parametrization can be used to calculate the matrix element corresponding to the NEEC process for a given partial wave component and a given multipolarity L, that yields [14]

$$\begin{aligned}
&\langle N^* I_d M_{I_d}, n_d \kappa_d m_d | H_{en} | N I_i M_{I_i}, \varepsilon \kappa m \rangle \\
&= \sum_{\mu=-L}^{L} (-1)^{I_d + M_{I_i} + L + \mu + m + 3j_d} R_0^{-(L+2)} R_{L,\kappa_d,\kappa} \langle N^* I_d \| Q_L \| N I_i \rangle \\
&\times \sqrt{2j_d+1} \sqrt{\frac{4\pi}{(2L+1)^3}} C(I_i I_d L; -M_{I_i} M_{I_d} \mu) \\
&\times C(j j_d L; -m m_d - \mu) C\left(j_d L j; \frac{1}{2} 0 \frac{1}{2}\right),
\end{aligned} \tag{40}$$

where Q_{LM} is the electric multipole moment defined by [17]

$$Q_{LM} = \int d^3 r_n r_n^L Y_{LM}(\theta_n, \varphi_n) \rho_n(\vec{r}_n). \tag{41}$$

The electronic radial integral is given by

$$\begin{aligned}
R_{L,\kappa_d,\kappa} = &\frac{1}{R_0^{L-1}} \int_0^{R_0} dr r^{L+2} \left[f_{n_d \kappa_d}(r) f_{\varepsilon\kappa}(r) + g_{n_d \kappa_d}(r) g_{\varepsilon\kappa}(r) \right] \\
&+ R_0^{L+2} \int_{R_0}^{\infty} dr r^{-L+1} \left[f_{n_d \kappa_d}(r) f_{\varepsilon\kappa}(r) + g_{n_d \kappa_d}(r) g_{\varepsilon\kappa}(r) \right]
\end{aligned} \tag{42}$$

with $g_{\varepsilon\kappa}(r)$ and $f_{\varepsilon\kappa}(r)$ being the large and small radial components of the relativistic continuum electron partial wave function

$$\Psi_{\varepsilon\kappa m}(\vec{r}) = \begin{pmatrix} g_{\varepsilon\kappa}(r) \Omega_{\kappa}^m(\theta,\varphi) \\ i f_{\varepsilon\kappa}(r) \Omega_{-\kappa}^m(\theta,\varphi) \end{pmatrix}, \tag{43}$$

with the spherical spinor functions Ω_{κ}^m, and $g_{n_d\kappa_d}(r)$ and $f_{n_d\kappa_d}(r)$ the radial components of the bound Dirac wave function.

For the matrix element of the interaction Hamiltonian (12) between the nucleus and the radiation field, we follow the outline in Ref. [23], considering that the wavelength of the radiation is large compared to the nuclear radius, $kR_0 \ll 1$, so that the spherical Bessel functions can be approximated in the first order in kr as

$$j_L(kr) \simeq \frac{(kr)^L}{(2L+1)!!}. \tag{44}$$

In this case the electric solution of the wave equation can be written as

$$\vec{A}_{(e)kLM}(\vec{r}) = -\sqrt{\frac{4\pi c k}{R}} \frac{\sqrt{(L+1)(2L+1)}}{(2L+1)!!} (kr)^{L-1} \vec{Y}_{LL-1}^M(\theta,\varphi). \tag{45}$$

With the use of the continuity equation for the nuclear current $\vec{j}_n$ we obtain for the matrix element

$$\langle N I_i M_{I_i}, (e) kLM | H_{nr} | N^* I_d M_{I_d}, 0 \rangle = (-1)^{I_d - M_{I_d} + 1} \sqrt{\frac{4\pi c k}{R}} C(I_i I_d L; M_{I_i} - M_{I_d} M) \times \frac{\sqrt{L+1}}{\sqrt{L(2L+1)}} \frac{i k^L}{(2L+1)!!} \langle N I_i \| Q_L \| N^* I_d \rangle. \tag{46}$$

The remaining matrix element of H_{er} can be evaluated by writing the electric solution of the wave equation in Eq. (9) in a more suitable form. Using the properties of the vector spherical harmonics [24] we obtain

$$\vec{A}_{(e)kLM}(\vec{r}) = \sqrt{\frac{4\pi c k}{R}} \left(\sqrt{\frac{L}{2L+1}} j_{L+1}(kr) \vec{Y}_{LL+1}^M(\theta,\varphi) - \sqrt{\frac{L+1}{2L+1}} j_{L-1}(kr) \vec{Y}_{LL-1}^M(\theta,\varphi) \right). \tag{47}$$

The electron-radiation interaction matrix element then yields

$$\langle n_d\kappa_d m_d,(e)kLM|H_{er}|\varepsilon\kappa m,0\rangle = -\sqrt{\frac{4\pi ck}{R}}\left(\sqrt{\frac{L}{2L+1}}\langle n_d\kappa_d m_d|j_{L+1}(kr)\vec{\alpha}\cdot\vec{Y}^M_{LL+1}(\theta,\varphi)|\varepsilon\kappa m\rangle\right.$$
$$\left. -\sqrt{\frac{L+1}{2L+1}}\langle n_d\kappa_d m_d|j_{L-1}(kr)\vec{\alpha}\cdot\vec{Y}^M_{LL-1}(\theta,\varphi)|\varepsilon\kappa m\rangle\right). \tag{48}$$

The matrix elements containing the product of the spherical Bessel spherical functions, the Dirac matrix $\vec{\alpha}$, and the vector spherical harmonics can be expressed in a compact way using the properties of the spherical tensor operators [25]. The expression in the above equation becomes

$$\langle n_d\kappa_d m_d,(e)kLM|H_{er}|\varepsilon\kappa m,0\rangle = i(-1)^{j-L+\frac{1}{2}}\sqrt{\frac{4\pi ck}{R}}C(jLj_d;mMm_d)\sqrt{\frac{2j+1}{4\pi}}\begin{pmatrix} j_d & j & L \\ \frac{1}{2} & -\frac{1}{2} & 0\end{pmatrix}$$
$$\times\left[\sqrt{\frac{L+1}{L(2L+1)}}[LI^-_{L-1}-(\kappa_d-\kappa)I^+_{L-1}] + \sqrt{\frac{L}{(L+1)(2l+1)}}[(L+1)I^-_{L+1}+(\kappa_d-\kappa)I^+_{L+1}]\right], \tag{49}$$

with the radial integrals [25]

$$I^{\pm}_L = \int_0^\infty drr^2 j_L(kr)\left[g_{n_d\kappa_d}(r)f_{\varepsilon\kappa}(r)\pm g_{\varepsilon\kappa}(r)f_{n_d\kappa_d}(r)\right]. \tag{50}$$

Combining the formulas of the three matrix elements from Eqs. (40), (46), and (49) in the expression of the Fano profile parameter $Q_f^{(e)}$ and using the summation properties of the Clebsch-Gordan coefficients we obtain the final formula

$$\frac{1}{Q_f^{(e)}} = \pi\rho_i(-1)^{3I_d+I_i+1}R_0^{-(L+2)}(2j_d+1)\sqrt{\frac{L}{(L+1)(2L+1)^3}}k^{-L}(2L+1)!!\sum_\kappa R_{L,\kappa_d,\kappa}(2j+1)\begin{pmatrix} j_d & j & L \\ \frac{1}{2} & -\frac{1}{2} & 0\end{pmatrix}^2$$
$$\times\left[\sqrt{\frac{L+1}{L(2L+1)}}[LI^-_{L-1}-(\kappa_d-\kappa)I^+_{L-1}] + \sqrt{\frac{L}{(L+1)(2L+1)}}[(L+1)I^-_{L+1}+(\kappa_d-\kappa)I^+_{L+1}]\right]. \tag{51}$$

C. Magnetic transitions

The magnetic transitions in the nucleus can be easily included in the calculation by assuming that the electron does not penetrate the nucleus, i.e., that the electronic radial coordinate r_e is always larger than the nuclear radial coordinate r_n. This approximation is precise enough for the studied cases [26,27]. The NEEC matrix element for the magnetic transition, involving only the magnetic Hamiltonian H_{magn} for a given partial wave and a given multipolarity can be written as [14]

$$\langle N^*I_dM_{I_d},n_d\kappa_d m_d|H_{\text{magn}}|NI_iM_{I_i},\varepsilon\kappa m\rangle = 4\pi i\sqrt{\frac{L+1}{L(2L+1)^3}}\sum_{\mu=-L}^{L}(-1)^{I_i-M_{I_i}+\mu+1}C(I_dI_iL;M_{I_d}-M_{I_i}\mu)\langle N^*I_d||M_L||NI_i\rangle$$
$$\times\langle n_d\kappa_d m_d|r^{-(L+1)}\vec{\alpha}\cdot\vec{Y}^{-\mu}_{LL}(\theta,\varphi)|\varepsilon\kappa m\rangle, \tag{52}$$

where the electronic matrix element can be evaluated in a similar way as the ones in Eq. (49) to yield

$$\langle n_d\kappa_d m_d|r^{-(L+1)}\vec{\alpha}\cdot\vec{Y}^{-\mu}_{LL}(\theta,\varphi)|\varepsilon\kappa m\rangle = i(-1)^{j-L+1/2}\sqrt{\frac{(2j+1)(2L+1)}{4\pi L(L+1)}}C(jLj_d;m-\mu m_d)(\kappa_d+\kappa)\begin{pmatrix} j_d & j & L \\ \frac{1}{2} & -\frac{1}{2} & 0\end{pmatrix}$$
$$\times\int_0^\infty drr^{-L+1}[g_{n_d\kappa_d}(r)f_{\varepsilon\kappa}(r)+f_{n_d\kappa_d}(r)g_{\varepsilon\kappa}(r)]. \tag{53}$$

This way of writing the electronic matrix element is equivalent to the more lengthy one presented previously in Ref. [14].

Now let us consider the matrix element corresponding to RR. It has, up to the presence of the spherical Bessel functions, a similar expression

$$\langle n_d\kappa_d m_d,(m)kLM|H_{er}|\varepsilon\kappa m,0\rangle = -\sqrt{\frac{4\pi ck}{R}}\langle n_d\kappa_d m_d|j_L(kr)\vec{\alpha}\cdot\vec{Y}^M_{LL}(\theta,\varphi)|\varepsilon\kappa m\rangle. \tag{54}$$

Using the properties of the spherical tensor operators [25], we can write the RR matrix element as

$$\langle n_d\kappa_d m_d,(m)kLM|H_{er}|\varepsilon\kappa m,0\rangle = \sqrt{\frac{4\pi ck}{R}}i(-1)^{j-L-\frac{1}{2}}\sqrt{\frac{(2j+1)(2L+1)}{4\pi L(L+1)}}C(jLj_d;mMm_d)(\kappa_d+\kappa)\begin{pmatrix} j_d & j & L \\ \frac{1}{2} & -\frac{1}{2} & 0\end{pmatrix}$$
$$\times\int_0^\infty dr j_L(kr)\left[g_{n_d\kappa_d}(r)f_{\varepsilon\kappa}(r)+f_{n_d\kappa_d}(r)g_{\varepsilon\kappa}(r)\right]. \tag{55}$$

The remaining matrix element involved in the expression of the Fano profile parameter Q_f is that of the interaction between the nucleus and the radiation field (12). We make use again of the long-wavelength approximation, so that the spherical Bessel functions are written as in Eq. (44). With this approximation and using the properties of the vector spherical harmonics, the magnetic solution of the wave equation can be expressed as

$$\vec{A}_{(m)kLM}(\vec{r}) = \sqrt{\frac{4\pi ck}{R}}\frac{k^L}{i\sqrt{L(L+1)}}\frac{1}{(2L+1)!!}$$
$$\times(\vec{r}\times\vec{\nabla})[r^L Y_{LM}(\theta,\varphi)]. \tag{56}$$

Rewriting the Hamiltonian H_{nr} we obtain

$$H_{nr} = i\sqrt{\frac{4\pi ck}{R}}\sqrt{\frac{L+1}{L}}\frac{k^L}{(2L+1)!!}\frac{1}{c(L+1)}$$
$$\times\int d^3r_n[\vec{r}_n\times\vec{j}_n(\vec{r}_n)]\cdot\vec{\nabla}[r_n^L Y_{LM}(\theta_n,\varphi_n)]. \tag{57}$$

The integral over the nuclear coordinate can be related to the magnetic multipole operator M_{LM}, defined as [17]

$$M_{LM} = \frac{1}{c(L+1)}\int d^3r_n[\vec{r}_n\times\vec{j}_n(\vec{r}_n)]\cdot\vec{\nabla}[r_n^L Y_{LM}(\theta_n,\varphi_n)]. \tag{58}$$

The matrix element of the interaction Hamiltonian between the radiation field and the nucleus yields

$$\langle NI_iM_{I_i},(m)kLM|H_{nr}|N^*I_dM_{I_d},0\rangle$$
$$= \sqrt{\frac{4\pi ck}{R}}\frac{ik^L}{\sqrt{L}}\frac{\sqrt{L+1}}{(2L+1)!!}\langle NI_iM_{I_i}|M_{LM}|N^*I_dM_{I_d}\rangle$$
$$= (-1)^{I_d-M_{I_d}}\sqrt{\frac{4\pi ck}{R}}\frac{ik^L}{(2L+1)!!}\sqrt{\frac{L+1}{L(2L+1)}}$$
$$\times C(I_dI_iL;M_{I_d}-M_{I_i}-M)\langle NI_i\|M_L\|N^*I_d\rangle. \tag{59}$$

Combining the results from Eqs. (52), (55), and (59) we write the expression of the dimensionless Fano profile parameter $Q_f^{(m)}$, making use of the summation properties of the Clebsch-Gordan coefficients

$$\frac{1}{Q_f^{(m)}} = \frac{\pi\rho_i(-1)^{I_i+3I_d+1}(2j_d+1)}{L(2L+1)(L+1)}k^{-L}(2L+1)!!\sum_\kappa(2j+1)$$
$$\times(\kappa_d+\kappa)^2\int_0^\infty drr^{-L+1}[g_{n_d\kappa_d}(r)f_{\varepsilon\kappa}(r)+f_{n_d\kappa_d}(r)g_{\varepsilon\kappa}(r)]$$
$$\times\begin{pmatrix} j_d & j & L \\ \frac{1}{2} & -\frac{1}{2} & 0\end{pmatrix}^2\int_0^\infty dr j_L(kr)[g_{n_d\kappa_d}(r)f_{\varepsilon\kappa}(r)$$
$$+f_{n_d\kappa_d}(r)g_{\varepsilon\kappa}(r)]. \tag{60}$$

III. NUMERICAL RESULTS

We have calculated the Fano profile parameter and the interference cross section term $\sigma_{\rm int}$ as a function of the incoming electron energy for several collision systems involving electric $E2$ and magnetic $M1$ transitions. We consider suitable cases of isotopes which have energetically low-lying nuclear levels which make the interference between NEEC and RR possible.

For the case of the electric transitions we consider the $0^+\rightarrow 2^+$ $E2$ transitions of the $^{236}_{92}$U, $^{238}_{92}$U, $^{248}_{96}$Cm, $^{174}_{70}$Yb, $^{170}_{68}$Er, $^{154}_{64}$Gd, $^{156}_{64}$Gd, $^{162}_{66}$Dy, and $^{164}_{66}$Dy even-even nuclei. The energies of the excited nuclear levels $E_{\rm exc}$ as well as the reduced transition probabilities $B(E2)$, that are needed for the calculation of the natural width of the nuclear excited state and the NEEC cross section and rate, are taken from Ref. [28]. The natural width of the nuclear excited state is considered to be the sum of the partial radiative rates $A_r^{d\rightarrow f}$ and the IC rates $A_{\rm IC}^d$,

$$\Gamma_d = \sum_f A_r^{d\rightarrow f} + \sum_i A_{\rm IC}^{d\rightarrow i}. \tag{61}$$

Here we sum the radiative transition rates to all possible final states (note that in our case there is only one nuclear final state, namely, the ground state). By summing over i we account for internal conversion to the initial state of the NEEC process and all other possible IC channels, for the case when the capture occurs into a He-like ion. The IC rate can be related to the NEEC rate through the principle of detailed balance

TABLE I. Parameters of the NEEC total cross section and the interference term for various heavy ion collision systems involving electric quadrupole transitions. E_{exc} denotes the nuclear excitation energy, E_c is the continuum electron energy at resonance, Y_n stands for the resonant recombination rate, and Γ_d is the total width of the excited nuclear state. The column denoted by S contains the NEEC resonance strengths, $1/Q_f$ is the inverse Fano line profile parameter, and R^{int} stands for the profile asymmetry parameter. See the text for further explanations.

Isotope	E_{exc}(keV)	E_c(keV)	Orbital	$Y_n(1/s)$	Γ_d(eV)	S(b eV)	$1/Q_f$	R^{int}
$^{164}_{66}$Dy	73.392	10.318	$1s_{1/2}$	1.86×10^{8}	4.37×10^{-8}	3.88×10^{-2}	-2.11×10^{-3}	3.67×10^{-3}
$^{170}_{68}$Er	78.591	11.350	$1s_{1/2}$	2.23×10^{8}	5.75×10^{-8}	4.70×10^{-2}	-2.07×10^{-3}	4.05×10^{-3}
$^{174}_{70}$Yb	76.471	4.897	$1s_{1/2}$	1.79×10^{8}	4.85×10^{-8}	9.27×10^{-2}	-2.09×10^{-3}	4.30×10^{-3}
$^{154}_{64}$Gd	123.071	64.005	$1s_{1/2}$	5.69×10^{8}	2.51×10^{-7}	2.91×10^{-2}	-2.61×10^{-4}	8.77×10^{-4}
$^{156}_{64}$Gd	88.966	74.742	$2s_{1/2}$	3.35×10^{7}	1.21×10^{-7}	7.09×10^{-4}	-6.10×10^{-5}	1.67×10^{-3}
$^{156}_{64}$Gd	88.966	74.896	$2p_{1/2}$	1.16×10^{8}	1.32×10^{-7}	2.25×10^{-3}	-1.16×10^{-5}	1.00×10^{-4}
$^{156}_{64}$Gd	88.966	75.680	$2p_{3/2}$	1.59×10^{8}	1.27×10^{-7}	3.17×10^{-3}	3.06×10^{-4}	1.86×10^{-3}
$^{162}_{66}$Dy	80.660	65.432	$2s_{1/2}$	2.81×10^{7}	9.39×10^{-8}	6.25×10^{-4}	-1.28×10^{-4}	3.26×10^{-3}
$^{162}_{66}$Dy	80.660	66.594	$2p_{1/2}$	1.59×10^{8}	1.11×10^{-7}	2.98×10^{-3}	-5.78×10^{-5}	3.06×10^{-4}
$^{162}_{66}$Dy	80.660	66.492	$2p_{3/2}$	2.15×10^{8}	1.04×10^{-7}	4.24×10^{-2}	3.56×10^{-4}	1.31×10^{-3}
$^{236}_{92}$U	45.242	12.404	$2s_{1/2}$	1.06×10^{8}	1.76×10^{-8}	8.47×10^{-3}	1.60×10^{-3}	2.00×10^{-3}
$^{236}_{92}$U	45.242	12.698	$2p_{1/2}$	3.02×10^{9}	4.01×10^{-7}	1.02×10^{-2}	-1.26×10^{-3}	1.27×10^{-3}
$^{236}_{92}$U	45.242	16.871	$2p_{3/2}$	3.10×10^{9}	2.07×10^{-7}	1.52×10^{-2}	-9.86×10^{-4}	5.01×10^{-4}
$^{238}_{92}$U	44.910	12.073	$2s_{1/2}$	1.11×10^{8}	1.81×10^{-8}	8.80×10^{-3}	1.61×10^{-3}	2.01×10^{-3}
$^{238}_{92}$U	44.910	12.356	$2p_{1/2}$	3.14×10^{9}	4.17×10^{-7}	1.06×10^{-2}	-1.24×10^{-3}	1.25×10^{-3}
$^{238}_{92}$U	44.910	16.534	$2p_{3/2}$	3.23×10^{9}	2.16×10^{-7}	1.56×10^{-2}	-9.97×10^{-4}	5.07×10^{-4}
$^{248}_{96}$Cm	43.380	6.888	$2s_{1/2}$	2.18×10^{8}	3.25×10^{-8}	1.78×10^{-2}	1.92×10^{-3}	2.16×10^{-3}
$^{248}_{96}$Cm	43.380	7.190	$2p_{1/2}$	5.47×10^{9}	7.24×10^{-7}	1.91×10^{-2}	-5.96×10^{-4}	5.99×10^{-4}
$^{248}_{96}$Cm	43.380	12.356	$2p_{3/2}$	5.33×10^{9}	3.54×10^{-7}	2.20×10^{-2}	-1.43×10^{-3}	7.24×10^{-4}

$$A_{\mathrm{IC}}^{d\to i}=\frac{2(2I_i+1)}{(2I_d+1)(2j_d+1)}Y_n^{i\to d}. \tag{62}$$

The NEEC rates and cross sections are calculated using an improved version of the computer routines applied in Ref. [14]. We consider the capture into the bare ions of $^{164}_{66}$Dy, $^{170}_{68}$Er, $^{174}_{70}$Yb, and $^{154}_{64}$Gd. For the cases of the U isotopes and for $^{248}_{96}$Cm, the capture into the K shell is not possible due to the low energy level of the first excited nuclear state. For these three systems, recombination into the L shell of initially He-like ions is the most probable one. We regard the capture of the electron into a closed shell configuration as a one-electron problem, without the participation of the K-shell electrons. We also consider the capture of the electron into the He-like ions of $^{156}_{64}$Gd and $^{162}_{66}$Dy, in which case the width of the nuclear excited state in Eq. (61) contains partial IC rates accounting for the possible IC of the K-shell electrons.

A numerical evaluation of the radial integrals corresponding to NEEC [$R_{L,\kappa_d,\kappa}$, see Eq. (42)] and the ones corresponding to RR [$I^{\pm}_{L\pm1}$, Eq. (50)] is needed for the calculation of the Fano profile parameters and for the interference cross sections. We consider Coulomb-Dirac wave functions for the continuum electron and wave functions calculated with the GRASP92 package [29] by considering a homogeneously charged nucleus for the bound electron. In the case of recombination into the He-like ions we assume a total screening of the nuclear charge for the continuum electron, i.e., we use Coulomb-Dirac functions with an effective nuclear charge $Z_{\mathrm{eff}}=Z-2$. For the bound electron wave functions, the electron-electron interaction is accounted for in the Dirac-Fock approximation. The value of $R_{L,\kappa_d,\kappa}$ is not affected by finite nuclear size effects on the accuracy level of our calculations. Nevertheless, the finite size of the nucleus has a sensitive effect on the energy levels of the bound electron. The energy of the bound electronic state is calculated with GRASP92 and includes one-loop one-electron quantum electrodynamic terms, and in the case of many-electron bound states approximate QED screening corrections. The nuclear radius R_0 is calculated according to the semiempirical formula [30]

$$R_0=(1.0793A^{1/3}+0.73587)\ \mathrm{fm}, \tag{63}$$

where A is the atomic mass number. Values of the Fano profile parameters, as well as the NEEC rate and natural width of the nuclear excited state are presented in Table I. The values of the resonance strength of NEEC, given in Ref. [14],

$$S_d=\frac{2\pi^2}{p^2}\frac{A_r^{d\to f}Y_n^{i\to d}}{\Gamma_d}, \tag{64}$$

are also presented.

The Fano line profile parameter characterizes the strength of the interference effects between the two recombination

channels. Smaller values of $|Q_f|$ indicate more pronounced interference. A more quantitative measure of the interference is defined in Ref. [31] as the ratio of the interference term and the resonant process term at the energy $\varepsilon_{\pm 1/2}=E_d \pm \Gamma_d/2$,

$$R^{\mathrm{int}} = \left| \frac{\sigma_{\mathrm{int}}(\varepsilon_{\pm 1/2})}{\sigma_{\mathrm{NEEC}}(\varepsilon_{\pm 1/2})} \right| = \frac{\Gamma_d}{Y_n^{i\to d}} \frac{2I_d+1}{2I_i+1} \frac{1}{|Q_f|}. \quad (65)$$

Values for this line asymmetry parameter R^{int} are given in the last column of Tables I and III.

A possibility to cross-check the numerical accuracy of the present calculations is given by the matrix element of the interaction Hamiltonian H_{er}, which enters the expression of the Fano profile parameter. We can use the matrix element to calculate the total cross section for RR for a given energy, which can be written in the spherical wave approach as

$$\sigma_{\mathrm{RR}} = \frac{2\pi}{F_i} \frac{1}{2} \sum_{m_s} \frac{1}{4\pi} \int d\Omega_p \sum_{m_d} \sum_{\lambda LM} \times |\langle n_d \kappa_d m_d, \lambda k LM | H_{er} | \vec{p} m_s, 0 \rangle|^2 \rho_f. \quad (66)$$

RR cross sections calculated by this formula and with the radial wave functions described above reproduce the values tabulated in Ref. [20] with a typical relative accuracy of about one per thousand, as it can be seen in Table II.

For the magnetic multipole transitions we consider the $M1$ transitions of the odd isotopes $^{165}_{67}$Ho, $^{173}_{70}$Yb, $^{55}_{25}$Mn, $^{57}_{26}$Fe, $^{40}_{19}$K, $^{155}_{64}$Gd, $^{157}_{64}$Gd, $^{185}_{75}$Re, and $^{187}_{75}$Re. Numerical results for these ions are presented in Table III. We present NEEC rates and resonance strengths with improved accuracy with respect to our previous results [14]. The electronic radial integrals are calculated numerically using the same type of wave functions for the bound and continuum electron as for the electric transitions. The reduced magnetic transition probability $B(M1)$ and the energies of the nuclear levels are taken from Refs. [32–40]. Recombination into the K shell is possible for all the chosen ions, except for Gd. We also present results for recombination into the initially He-like ions of the $^{155}_{64}$Gd and $^{157}_{64}$Gd isotopes.

In Fig. 2 interference and scaled NEEC cross section terms are plotted as a function of the continuum electron energy for the $M1$ transition of $^{185}_{75}$Re and $E2$ transition of $^{174}_{70}$Yb, respectively. These are the isotopes with the largest values for the resonance strengths for the magnetic and electric multipole transitions, respectively. The NEEC cross section has the shape of a very narrow Lorentzian, with the width given by the natural width of the excited nuclear state, about 2.4×10^{-5} eV for the case of $^{185}_{75}$Re and 4.9×10^{-8} eV for the case of $^{174}_{70}$Yb. The interference term σ_{int} for both electric and magnetic cases is more than two orders of magnitude smaller than the NEEC terms σ_{NEEC}. The magnitude of the interference term can be explained by investigating the contributions of the multipolarities that enter the RR cross section σ_{RR}. While σ_{RR} consists of an infinite sum of multipolarities, in the interference process only the RR photon with the multipolarity of the nuclear transition participates. The main contribution to the RR cross section comes from the electric dipole photon. The cross sections corresponding to the $M1$ and $E2$ photons are considerably smaller. In the case of $^{174}_{70}$Yb, the $E2$ multipole accounts for only 121 b in the total RR cross section of 2080 b, while the $M1$ multipole for $^{185}_{75}$Re only contributes 0.5 b to the total RR cross section of 212 b.

TABLE II. Total RR cross sections for recombination into a given bound state of a bare ion, compared with results from Ref. [20]. The nuclear excitation energy E_{exc}, corresponding to the energy of the emitted photon, is given in the second column. The values from Ref. [20] are numerically interpolated by a spline routine to obtain the RR cross section at the resonance energy E_c.

				σ_{RR}(b)	
Isotope	E_{exc}(keV)	E_c(keV)	Orbital	This work	Ref. [20]
$^{164}_{66}$Dy	73.392	10.318	$1s_{1/2}$	832	832
$^{170}_{68}$Er	78.591	11.350	$1s_{1/2}$	797	795
$^{174}_{70}$Yb	76.471	4.897	$1s_{1/2}$	2080	2080
$^{154}_{64}$Gd	123.071	64.005	$1s_{1/2}$	79	79
$^{236}_{92}$U	45.242	11.113	$2s_{1/2}$	245	245
$^{236}_{92}$U	45.242	11.038	$2p_{1/2}$	295	294
$^{236}_{92}$U	45.242	15.601	$2p_{3/2}$	229	229
$^{238}_{92}$U	44.910	10.782	$2s_{1/2}$	252	253
$^{238}_{92}$U	44.910	10.706	$2p_{1/2}$	306	306
$^{238}_{92}$U	44.910	15.269	$2p_{3/2}$	236	236
$^{248}_{96}$Cm	43.380	5.500	$2s_{1/2}$	543	544
$^{248}_{96}$Cm	43.380	5.398	$2p_{1/2}$	768	769
$^{248}_{96}$Cm	43.380	11.018	$2p_{3/2}$	410	410
$^{165}_{67}$Ho	94.700	29.563	$1s_{1/2}$	252	252
$^{173}_{70}$Yb	78.647	7.073	$1s_{1/2}$	1410	1410
$^{185}_{75}$Re	125.358	42.198	$1s_{1/2}$	212	212
$^{187}_{75}$Re	134.243	51.083	$1s_{1/2}$	166	166
$^{55}_{25}$Mn	125.949	117.378	$1s_{1/2}$	0.865	0.849
$^{57}_{26}$Fe	14.412	5.135	$1s_{1/2}$	216	216
$^{40}_{19}$K	29.829	24.896	$1s_{1/2}$	6.64	6.55

As an electron energy resolution in the order of 10^{-5} eV and less can not be presently achieved in an experiment, we convolute the theoretical total cross section with the energy distribution of the electrons to give an orientation for measurements in near future. The energy distribution of the incoming electrons is assumed to be described by a Gaussian function with a width parameter s. The RR cross section has a practically constant value on the energy interval of s. In order to demonstrate the magnitude of the NEEC and interference cross sections σ_{NEEC} and σ_{int} compared to that of RR, we present in Fig. 3 the ratio of the convoluted cross sections

$$R(E,s) = \frac{\tilde{\sigma}_{\mathrm{NEEC}}(E,s) + \tilde{\sigma}_{\mathrm{int}}(E,s)}{\tilde{\sigma}_{\mathrm{RR}}(E,s)}, \quad (67)$$

in the case of $^{185}_{75}$Re as a function of the continuum electron energy for the three different experimental width parameters

TABLE III. Parameters of the NEEC total cross section and the interference term for various heavy ion collision systems involving magnetic dipole transitions. The notations are as defined in Table I.

Isotope	E_{exc}(keV)	E_c(keV)	Orbital	$Y_n(1/s)$	Γ_d(eV)	S(b eV)	$1/Q_f$	R^{int}
$^{165}_{67}$Ho	94.700	29.563	$1s_{1/2}$	1.28×10^{10}	1.17×10^{-5}	8.84×10^{-1}	-1.67×10^{-3}	2.90×10^{-3}
$^{173}_{70}$Yb	78.647	7.073	$1s_{1/2}$	7.32×10^{9}	4.80×10^{-6}	1.26	-2.24×10^{-3}	2.98×10^{-3}
$^{185}_{75}$Re	125.358	42.198	$1s_{1/2}$	2.62×10^{10}	2.36×10^{-5}	1.34	-2.58×10^{-3}	4.71×10^{-3}
$^{187}_{75}$Re	134.243	51.083	$1s_{1/2}$	2.50×10^{10}	2.47×10^{-5}	1.16	-2.50×10^{-3}	5.00×10^{-3}
$^{55}_{25}$Mn	125.949	117.378	$1s_{1/2}$	2.45×10^{7}	1.75×10^{-6}	9.22×10^{-4}	-2.14×10^{-5}	3.10×10^{-3}
$^{57}_{26}$Fe	14.412	5.135	$1s_{1/2}$	6.21×10^{6}	2.56×10^{-9}	1.19×10^{-3}	-6.73×10^{-5}	8.42×10^{-5}
$^{40}_{19}$K	29.829	24.896	$1s_{1/2}$	1.33×10^{7}	9.47×10^{-8}	2.27×10^{-3}	-1.46×10^{-5}	1.22×10^{-4}
$^{155}_{64}$Gd	60.008	45.784	$2s_{1/2}$	2.73×10^{8}	1.97×10^{-6}	3.18×10^{-3}	-1.25×10^{-4}	2.06×10^{-3}
$^{155}_{64}$Gd	60.008	45.938	$2p_{1/2}$	2.40×10^{7}	1.86×10^{-6}	2.94×10^{-4}	-1.85×10^{-5}	3.27×10^{-3}
$^{155}_{64}$Gd	60.008	46.722	$2p_{3/2}$	4.00×10^{6}	1.85×10^{-6}	4.84×10^{-5}	-1.81×10^{-5}	1.91×10^{-2}
$^{157}_{64}$Gd	54.533	40.309	$2s_{1/2}$	4.16×10^{8}	4.37×10^{-7}	2.86×10^{-2}	-1.25×10^{-4}	3.00×10^{-4}
$^{157}_{64}$Gd	54.533	40.463	$2p_{1/2}$	3.68×10^{7}	2.71×10^{-7}	4.07×10^{-3}	-2.00×10^{-5}	3.36×10^{-4}
$^{157}_{64}$Gd	54.533	41.247	$2p_{3/2}$	6.21×10^{6}	2.56×10^{-7}	7.12×10^{-4}	-1.94×10^{-5}	1.82×10^{-3}

$s=0.5$, 1, and 10 eV. While for a width parameter $s=0.5$ eV the contributions of the NEEC and interference terms can be clearly discerned from the RR background, for presently more realistic widths in the order of eVs or tens of eV the values of the ratio $R(E,s)$ are too small to be observed experimentally.

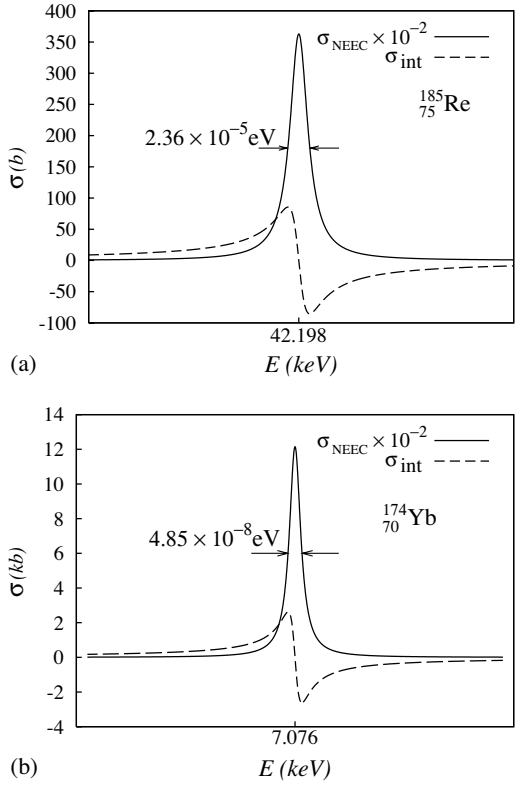

FIG. 2. Interference and NEEC terms of the cross section for capture into bare $^{185}_{75}$Re (upper figure) and bare $^{174}_{70}$Yb (lower figure) ions as a function of the continuum electron energy. The NEEC term is scaled by a factor of 10^{-2}.

IV. SUMMARY

In this article we investigated the interference between NEEC and RR in an electron recombination process. We derived the interference cross section and expressed it with the help of the dimensionless Fano profile parameter.

We calculated the interaction matrix elements for both electric and magnetic multipolarities using relativistic electronic wavefunctions. Nuclear excitations are described using a phenomenological nuclear collective model. The nuclear part of the matrix element is written by the help of the reduced nuclear transition probability whose value is taken from experimental works. For the quantization of the radiation field we use the multipole expansion.

Numerical values for the Fano profile parameters and interference cross sections were obtained for various heavy-ion collision systems. The interference term in the total cross

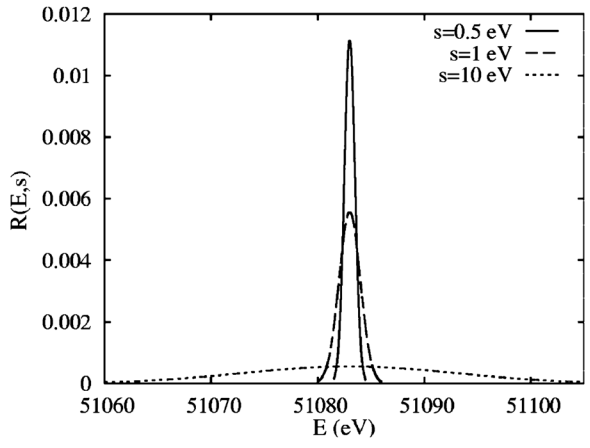

FIG. 3. The ratio $R(E,s)$ in Eq. (67) for recombination into bare $^{185}_{75}$Re as a function of the energy of the continuum electron for three different experimental electron energy width parameters s. See text for further explanations.

section of the recombination process is about two orders of magnitude smaller than the NEEC cross section. This is associated with the fact that from the infinite multipole expansion of the RR radiation, only the multipolarities corresponding to the type of nuclear transition interfere with the radiative decay photons following NEEC. The interference term has a narrow extent on the electron energy scale, which is related to the small natural width of the nuclear excited state. In order to simulate data of a recombination experiment, we convolute the total cross section with a Gaussian electron energy distribution of realistic width parameters. While for well-defined experimental electron energies the presence of NEEC could be discerned from the RR background, for larger width parameters both NEEC and the interference with RR become difficult to be observed experimentally.

If the angular distribution of the emitted photons in the radiative decay of the nucleus following NEEC is different from the one of the RR photons, this can be used to identify the resonant process in the RR background. Calculations investigating a possible NEEC signature in the angular distribution of the emitted photons are in progress.

ACKNOWLEDGMENTS

A.P. acknowledges the support from the Deutsche Forschungsgemeinschaft (DFG). This work is part of the doctoral thesis of A.P.

[1] A. Wolf *et al.*, Nucl. Instrum. Methods Phys. Res. A **441**, 183 (2000).
[2] A. J. González Martínez *et al.*, Phys. Rev. Lett. **94**, 203201 (2005).
[3] V. M. Shabaev, V. A. Yerokhin, T. Beier, and J. Eichler, Phys. Rev. A **61**, 052112 (2000).
[4] M. Zimmermann, N. Grün, and W. Scheid, J. Phys. B **30**, 5259 (1997).
[5] D. A. Knapp, P. Beiersdorfer, M. H. Chen, J. H. Scofield, and D. Schneider, Phys. Rev. Lett. **74**, 54 (1995).
[6] W. Spies *et al.*, Phys. Rev. Lett. **69**, 2768 (1992).
[7] V. Goldanskii and V. A. Namiot, Phys. Lett. **62B**, 393 (1976).
[8] T. Carreyre *et al.*, Phys. Rev. C **62**, 024311 (2000).
[9] S. Kishimoto, Y. Yoda, M. Seto, Y. Kobayashi, S. Kitao, R. Haruki, T. Kawauchi, K. Fukutani, and T. Okano, Phys. Rev. Lett. **85**, 1831 (2000).
[10] M. R. Harston and J. F. Chemin, Phys. Rev. C **59**, 2462 (1999).
[11] N. Cue, J.-C. Poizat, and J. Remillieux, Europhys. Lett. **8**, 19 (1989).
[12] J. C. Kimball, D. Bittel, and N. Cue, Phys. Lett. **152**, 367 (1991).
[13] Z.-S. Yuan and J. C. Kimball, Phys. Rev. C **47**, 323 (1993).
[14] A. Pálffy, W. Scheid, and Z. Harman, Phys. Rev. A **73**, 012715 (2006).
[15] S. Zakowicz, W. Scheid, and N. Grün, J. Phys. B **37**, 131 (2004).
[16] S. Zakowicz, Z. Harman, N. Grün, and W. Scheid, Phys. Rev. A **68**, 042711 (2003).
[17] P. Ring and P. Schuck, *The Nuclear Many-Body Problem* (Springer Verlag, New York, 1980).
[18] A. R. Edmonds, *Angular Momentum in Quantum Mechanics* (Princeton University Press, Princeton, 1996).
[19] J. Taylor, *Scattering Theory: The Quantum Theory of Nonrelativistic Collisions* (Wiley, New York, 1972).
[20] A. Ichihara and J. Eichler, At. Data Nucl. Data Tables **74**, 1 (2000).
[21] J. Eichler and W. Meyerhof, *Relativistic Atomic Collisions* (Academic Press, San Diego, 1995).
[22] W. Greiner and J. Maruhn, *Nuclear Models* (Springer Verlag, Berlin, 1996).
[23] J. Eisenberg and W. Greiner, *Nuclear Theory* (North-Holland, Amsterdam, 1987).
[24] D. Varshalovich, A. Moskalev, and V. Khersonskii, *Quantum Theory of Angular Momentum* (World Scientific, Singapore, 1988).
[25] I. P. Grant, J. Phys. B **7**, 1458 (1974).
[26] T. Green and M. Rose, Phys. Rev. **110**, 105 (1958).
[27] K. Alder, A. Bohr, T. Huus, B. Mottelson, and A. Winther, Rev. Mod. Phys. **28**, 432 (1956).
[28] S. Raman, C. Nestor, and P. Tikkanen, At. Data Nucl. Data Tables **78**, 1 (2001).
[29] F. A. Parpia, C. Froese-Fischer, and I. P. Grant, Comput. Phys. Commun. **94**, 249 (1996).
[30] W. R. Johnson and G. Soff, At. Data Nucl. Data Tables **33**, 405 (1985).
[31] E. Behar, V. L. Jacobs, J. Oreg, A. Bar-Shalom, and S. L. Hahn, Phys. Rev. A **62**, 030501(R) (2000).
[32] R. B. Firestone, Nucl. Data Sheets **62**, 159 (1991).
[33] V. S. Shirley, Nucl. Data Sheets **54**, 589 (1988).
[34] L. K. Peker, Nucl. Data Sheets **65**, 439 (1992).
[35] E. Browne, Nucl. Data Sheets **74**, 165 (1995).
[36] J. Huo, Nucl. Data Sheets **64**, 723 (1991).
[37] M. R. Bhat, Nucl. Data Sheets **67**, 195 (1992).
[38] J. A. Cameron and B. Singh, Nucl. Data Sheets **102**, 293 (2004).
[39] C. W. Reich, Nucl. Data Sheets **71**, 709 (1994).
[40] R. G. Hehner, Nucl. Data Sheets **55**, 71 (1988).